Dewetting of Low-Viscosity Films at Solid/Liquid Interfaces

Nicolas Péron, Françoise Brochard-Wyart, Hervé Duval

Dewetting of low-viscous films at solid/liquid interfaces

Nicolas Péron,[†,¶] Françoise Brochard-Wyart,[‡] and Hervé Duval[*,†]

Laboratoire de Génie des Procédés et Matériaux, Ecole Centrale Paris, France, and Institut Curie, Paris, France

E-mail: herve.duval@ecp.fr

Abstract

We report new experimental results on the dewetting of a mercury film (A) intercalated between a glass slab and an external non-miscible liquid phase (B), in conditions of large equilibrium contact angle. The viscosity of the external phase, η_B, was varied over seven orders of magnitude. We observe a transition between two regimes of dewetting at a threshold viscosity $\eta_B^* \approx (\rho_A e|\tilde{S}|)^{1/2}$, where ρ_A is the mercury density, e the film thickness and $|\tilde{S}|$ the effective spreading coefficient. For $\eta_B < \eta_B^*$, the regime is inertial. The velocity of dewetting is constant and ruled by Culick's law, $V \approx (|\tilde{S}|/(\rho_A e))^{1/2}$. Capillary waves were observed at high dewetting velocities : they are a signature of an hydraulic shock. For $\eta_B > \eta_B^*$, the regime is viscous. The dewetting velocity is constant and scales as $V \sim |\tilde{S}|/\eta_B$ in the limit of large η_B. We interpret this regime by a balance between the surface energy released during dewetting and the viscous dissipation in the surrounding liquid.

[*]To whom correspondence should be addressed
[†]LGPM, Ecole Centrale Paris
[‡]Institut Curie
[¶]Current address: Studec, Ivry-sur-Seine, France

Introduction

The dewetting of a liquid film deposited on a solid substrate in air is relatively well understood.[1] In partial wetting conditions, a macroscopic film of thickness e of liquid A on solid S is metastable below a critical thickness

$$e_c = 2\kappa^{-1}\sin(\theta_E/2), \tag{1}$$

where θ_E is the contact angle at equilibrium and $\kappa^{-1} = (\gamma_A/\rho_A g)^{1/2}$ is the capillary length (γ_A is the liquid surface tension, ρ_A its density and g the gravitational acceleration). It dewets as soon as a hole, larger than the critical nucleation radius, is made. Experiments show that, when the dry patch of radius R grows, the liquid is collected in a liquid rim which moves at constant velocity $V = dR/dt$ (see Fig. 1). Theoretically, the dewetting velocity can be derived by applying Newton's second law to the rim. The equation of motion reads (per unit length of the rim):

$$dP/dt = F_d - F_v, \tag{2}$$

where dP/dt is the variation of the rim momentum P per unit time, F_d is the driving force of the dewetting process and F_v is the dissipative force. F_d is equal to the effective spreading coefficient $|\tilde{S}|$ which takes into account both capillary and gravitational contributions:

$$\tilde{S} = S\left(1 - \frac{e^2}{{e_c}^2}\right), \tag{3}$$

where the conventional spreading coefficient S is given by $S = \gamma_S - (\gamma_A + \gamma_{AS})$ (γ_S is the surface energy of solid S and γ_{AS} is the A/S interfacial energy). Last, the force F_v scales as $F_v \sim \eta_A V/\theta_D$ (η_A is the dynamic viscosity of liquid A and θ_D is the so-called dynamic contact angle) if the viscous dissipation in liquid A dominates over all dissipation processes occurring during the dewetting. Depending on the film thickness e, two limiting behaviors can be distinguished, *i.e.*, the inertial regime,[2] when the viscous force F_v is small compared with the inertial term dP/dt, and the vis-

cous regime,[3] when F_v dominates. The thickness e^* characterizing the cross-over between the two regimes is given by $e^* \approx {\eta_A}^2/(\rho_A|S|)$. When $e \gg e^*$ (inertial regime) the dewetting velocity is given by:

$$V \approx (|\tilde{S}|/(\rho_A e))^{1/2} \tag{4}$$

This expression is formally identical to Culick's law describing soap film breakup.[4] When $e \ll e^*$, V scales as $V \sim |\tilde{S}|/\eta_A$. In the limit of small equilibrium contact angle $\theta_E \ll 1$ and small thickness $e \ll e_c$, the dewetting velocity in the viscous regime becomes:[3]

$$V \approx \frac{\gamma_A {\theta_E}^3}{k_A \eta_A} \tag{5}$$

where k_A is a logarithmic factor of the order of 10 and is due to the divergence of the dissipation in a wedge.[5] k_A involves the thickness of the native film, the width of the rim and a microscopic cutoff length depending on the nature of the liquid A.[1,6]

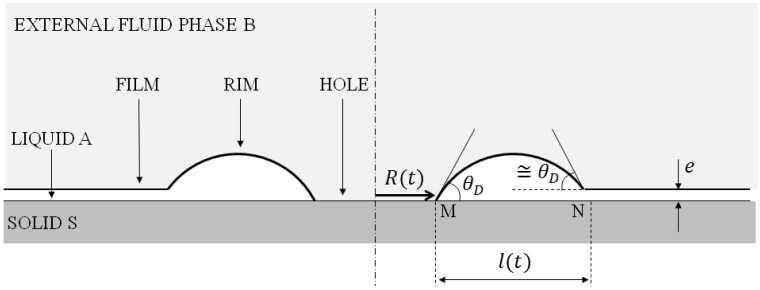

Figure 1: Sketch of the dewetting dynamics. The hole (of radius $R(t)$) in the intercalated film grows while the liquid is collected into a rim moving with velocity $V = dR/dt$.

While the dewetting of a liquid film lying between a solid and air is well documented, the dewetting of a liquid (A) film at the interface between a solid substrate (S) and an external liquid phase (B) has received little attention. In practice, the dewetting kinetics may significantly affect the efficiency of solid/liquid separation processes such as liquid metal refining. In that case, solid impurities called inclusions are removed from the liquid metal by capture at the interface between the liquid metal and a second non-miscible and more viscous liquid, *i.e.*, the slag. An inclusion

is definitely captured after the rupture and the subsequent dewetting of the liquid metal film that separates the inclusion from the slag.

Let us review the few investigations focusing on the dewetting dynamics in solid/liquid/liquid systems. The viscosity ratio of the liquid phases is denoted $\lambda = \eta_B/\eta_A$ and the contact angle θ_E is defined as the equilibrium contact angle of a drop of liquid A lying on solid S in the external phase B. According to our review, only the dewetting of viscous films has been investigated. We mean by a viscous film, a liquid film which dewets in the viscous regime whatever the viscous dissipation in the external phase is.

Shull and Karis[7] and Haidara *et al.*[8] studied solid/liquid/liquid systems characterized by a viscosity ratio, λ, much lower than 1. In this case, the dewetting should proceed as if the external phase is replaced by air.[9,10]

Shull and Karis[7] studied the dewetting of poly-ethylene-co-propylene (PEP) films on polystyrene (PS) or polymethylmethacrylate (PMMA) substrates immersed in a series of aliphatic alcohols (from C1 to C7). The viscosity of the pure PEP ($\eta_A = 1.4\ 10^{-1}$ Pa.s) was much larger than the viscosity of the alcohols (ranging from $\eta_B = 5.5\ 10^{-4}$ Pa.s for methanol to $\eta_B = 6.0\ 10^{-3}$ Pa.s for 1-heptanol). The PEP/alcohol interfacial energy ranged between 0.3 to 4.5 mN.m^{-1}. The alcohol phase was essentially used to induce the dewetting of the PEP film by changing the equilibrium contact angle of the PEP film from zero (in air) to some very large value (up to 180°). Shull and Karis observed circular dewetting patches whose radii, R, increased linearly with time. For the PS/PEP/alcohol system, characterized by an equilibrium contact angle lower than 180°, they found that the measured dewetting velocities concorded with Redon *et al.*'s law (Eq. 5). For the PMMA/PEP/alcohol system, characterized by an equilibrium contact angle of 180°, the dewetting velocities were found to scale as $V \sim |S|/\eta_A$. For both systems, the viscosity of the film, η_A, was taken as the viscosity of the alcohol saturated PEP instead of the viscosity of the pure PEP. Indeed the partial miscibility of alcohol (on the order of 10% for 1-butanol) in PEP could lead to a significant decrease in the viscosity (three-fold decrease in the case of 1-butanol).

Haidara *et al.*[8] investigated the dewetting of polydimethylsiloxane (PDMS) films (about 1μm

thick) on a non-wettable solid surface (hexadecyltrichlorosilane-treated silicone wafer) in pure water and in an aqueous surfactant solution (trisiloxane-ethylene oxide compound at the critical micelle concentration). The equilibrium contact angle was about 21° in pure water and about 46° in the surfactant solution. The interfacial energy between PDMS and pure water (resp. surfactant solution) was equal to 40 mN.m^{-1} (resp. 10 mN.m^{-1}). The viscosity of the PDMS oils varied between 10^{-2} Pa.s to 10 Pa.s and was much greater than the viscosity of the external aqueous phase (10^{-3} Pa.s). For the solid/PDMS/pure water system, the ${\eta_A}^{-1}$ dependence of the dewetting velocity was recovered after normalizing the velocities with the logarithmic factor.

Solid/liquid/liquid systems characterized by a viscosity ratio, λ, greater than 1 were investigated by Martin.[11] He studied the dewetting of a perfluoroalkoxy silicone oil (PFAS) film at the interface between a silanized glass slide and an external PDMS oil. PFAS (resp. PDMS) viscosity ranges from 0.4 to 20 Pa.s (resp. 30 to 2500 Pa.s), *i.e.*, viscosity ratio from 1.5 to 6250. The PFAS/PDMS interfacial energy was equal to 3.5 mN.m^{-1} and the spreading parameter S to about -3 mN.m^{-1}. Martin varied the film thickness, e, between 47 μm and 660 μm ($e \ll e_c$). He found that the dewetting velocity was independent of the film thickness and scales as $V \sim |S|{\eta_A}^{-0.4}{\eta_B}^{-0.6}$. He further established a model that accounts for his results. The main arguments are hereafter summarized: (i) the viscous friction in the film reads $F_v \sim \eta_A \theta^{-1} V$ whereas the friction in the external phase is given by the semi-empirical law[18] $F_v \sim \eta_B \theta^{0.7} V$; (ii) the dynamic contact angle adjusts in order to minimize the total dissipation in the film and in the external phase. It should be mentioned that Martin also investigated the dewetting of a liquid film intercalated between a silanized glass plate and a reticulated PDMS (soft rubber).[11,12] The radius of the dry patch R was found to increase with time according to $R(t) \sim t^{3/4}$. His results concord with the theoretical predictions of Brochard-Wyart and de Gennes[13] concerning the dewetting of a liquid film intercalated between a solid and a viscoelastic phase.

The present paper focuses on the dewetting of a low-viscosity film, lying between a solid and an external non-miscible viscous fluid. We mean by a low-viscosity film, a liquid film which tends to dewet in the inertial regime when the viscous dissipation in the external phase is negligible (as long

as $e \gg e^*$ and $e^* < e_c$). We expect two limiting dewetting behaviors depending on the viscosity of the external phase: (i) an inertial regime in the limit of small viscosity of the external phase η_B and (ii) a viscous regime for large enough values of η_B. It should be noted that the same retraction regimes, *i.e.*, inertial and viscous, were identified by Joanny and de Gennes[14] and Reyssat and Quéré[15] in the case of soap films and fluid films bursting in an external liquid phase. We chose to study experimentally the dewetting of a mercury film sandwiched between a glass slab and an external phase such as air, ethanol or a series of silicone oils. This system is characterized by (i) a low viscosity η_A, (ii) a large equilibrium contact angle θ_E, (iii) a large density ratio ρ_A/ρ_B and (iv) a strict immiscibility between the film phase and the external phase. These properties should make the analysis of the experiments easier and lead to simple asymptotic regimes.

In the following sections, we first describe our experimental device for observing the dewetting of a mercury film sandwiched between a glass slab and an external phase. Then, we report and discuss the experimental results. In particular, we present the variations of the dewetting velocities as a function of the film thickness and as a function of the external phase viscosity. Finally, we propose a model that accounts for the observed asymptotic behaviours.

Experimental methods

Solid/liquid/liquid system

The solid surface consisted of a slab of floated glass and the film phase was three-fold distilled mercury (purchased from Ophram Laboratoire, Saint-Fons, France). The glass slab, typically a square 40 mm in width, was fixed in the center of a cylindrical cell about 80 mm in internal diameter. The external phase varied from the ambient air to analytical grade ethanol and silicone oils with viscosities ranging from 3 10^{-3} to 100 Pa.s (CarlRoth's Silicone oil, M3 to M100000). Thus, the viscosity ratio between the external phase and the mercury film ($\eta_A = 1.55\ 10^{-3}$ Pa.s) varies between $\lambda = 10^{-2}$ (air) and $\lambda = 6\ 10^4$ (M100000 silicone oil). The density of the external liquid phase (*i.e.*, $\rho_B = 790$ kg.m^{-3} for ethanol and $\rho_B = 900$ to 980 kg.m^{-3} for M3 to M100000

at room temperature) is systematically one order smaller than the mercury density ($\rho_A = 13600$ kg.m^{-3}). The capillary data on the liquid phases are compiled in Tab. 1. It should be noted that the capillary data reported for the silicone oils correspond to high-viscosity ones, the surface tension of the low-viscosity silicone oils may be slightly lower (down to 19 N.m^{-1} for M3).

Table 1: Interfacial tensions A/B, surface tension of B, contact angle of B lying on S in the air, contact angle of A lying on S in external phase B, spreading coefficient, capillary length, critical thickness for different three-phases combinations of an external fluid phase (B) with mercury (A) and glass (S). The tabulated angles are averages of the advancing and the receding static contact angles.
[a] Ref.[16]
[b] Ref.[17]
[c] Ref.[18]
[d] Ref.[1]
[e] Ref.[19]
[f] Calculated from the thermodynamic equation:[20] $\gamma_{AB}\cos\theta_{AB} = \gamma_A\cos\theta_A - \gamma_B\cos\theta_B$.

External phase B	γ_{AB} (N.m^{-1})	γ_B (N.m^{-1})	θ_B (deg)	θ_{AB} (deg)	S (N.m^{-1})	κ^{-1} (10^{-3}m)	e_c (10^{-3}m)
air	0.486[a]	-	-	138[a]	-0.85	1.91	3.58
ethanol	0.389[a]	0.0224	34[b]	167.5[f]	-0.77	1.76	3.52
silicone oil	0.425[e]	0.0215[d]	48[c]	152[f]	-0.80	1.86	3.60

Tab. 1 shows that the equilibrium contact angle of mercury on glass surrounded by air, ethanol or silicone oil is systematically large and the spreading parameters, $S = \gamma_{BS} - (\gamma_{AB} + \gamma_{AS})$, are negative and narrow within 10%. The critical thickness e_c of film metastability is given by Eq. 1 where the capillary length reads $\kappa^{-1} = \left(\frac{\gamma_{AB}}{(\rho_A - \rho_B)g}\right)^{1/2}$. It is equal to about 3.5 mm for air, ethanol or silicone oil. The theoretical thickness characterizing the crossover between inertial and viscous dewetting of mercury intercalated between glass and air is very small, *i.e.*, in the range of nanometers, which means that the dewetting of a macroscopic mercury film between glass and air is never viscous.

Experimental set-up

The dewetting velocity in our experiments was measured as commonly from video recordings (using a high-speed camera Phantom v310, Vision Research, Ametek, together with a Sigma 105 mm

F2.8 EX DG Macro objective), while the film thickness was tuned and measured by a gravimetric procedure. The experimental setup is sketched in Fig. 2.

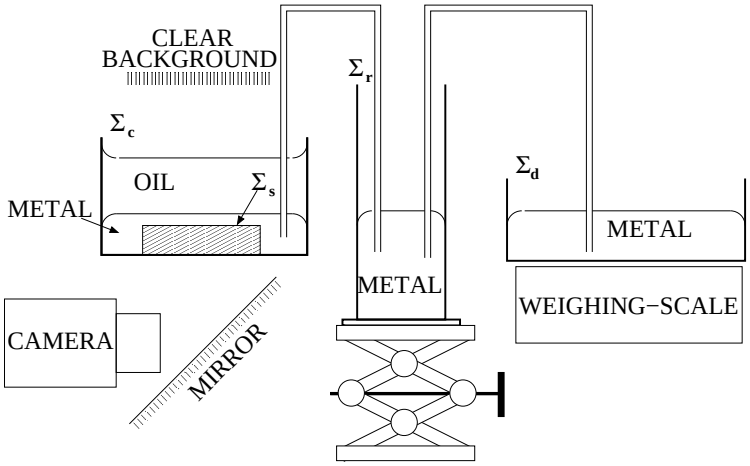

Figure 2: Experimental setup.

The cell where the glass slab was fixed had a transparent glass bottom allowing video recording from underneath, clear from any distortion related to a deformation of the external phase/air interface in the course of the dewetting. This cell was set on a frame that was orientated around two perpendicular horizontal axes under the control of a goniometer. The slab surface was oriented horizontally to within $\pm$ 0.06° using a laser beam reflected and projected onto a screen several meters away. The goniometer was tuned as the projected spot to coincide with that of the same beam when reflected onto a liquid surface instead of the glass slab.

The glass slab cell was filled with mercury and then set to communicate through siphons to two vessels: a reservoir of mercury mounted on a vertical stage allowing to tune the level of liquid and another dish set on a digital weighing scale. The mercury level was first set as to amply cover the surface of the glass slab. Then the external fluid phase was gently poured into the cell. The thickness of the resulting external phase layer was 30$\pm$1 mm in all experiments. Next, the mercury level was carefully decreased to sub-millimeter thickness by moving the above mentioned mercury reservoir vertically. The native film thickness ranges typically between 0.4 mm and 1.2 mm (the range was larger for ethanol as the external phase, *i.e.*, from 0.4 mm to 2.5 mm, and was narrower for M3 and M100000 silicone oils). We emphasize that the external phase thickness is much greater

than the thickness of the mercury film: in this condition, we expect that the dewetting dynamics slightly depend on the external phase thickness.

To initiate a hole in the mercury film, a plastic rod was introduced as follows: first, it was immersed vertically into the external phase so that its tip reached the surface of the mercury. A settling time, up to 1 hour for the most viscous oil, was then observed for the system to reach hydrostatic equilibrium. Then the mercury film was perforated until dewetting occurred by moving the rod further down.

The dewetting process was filmed at recording speeds ranging from 24 frames per second to 6000 frames per second depending on the dewetting velocity, which roughly varied between 5 10^{-4} $m.s^{-1}$ (for the most viscous silicone oil) and 0.2 $m.s^{-1}$ (for the thinner films in inertial regime).

The initial thickness of the film was calculated *a posteriori* as a function of the difference Δm in weighing scale reading before and after the dewetting. A settling time up to 20 min was necessary before the weigh scale reading reached the static value related to the new hydrostatic equilibrium. The expressions leading to the thickness e of the film are given in the appendix. It should be noted that the meniscus at the edge of the glass slab was taken into account in the calculation. The uncertainty over film thickness was a few percent (typically 3%).

Finally, the hole radius was measured automatically from the video records by a Matlab image treatment code: for each image, coordinates of points on the edge of the hole are determined by the Sobel method. A circle is then fitted onto the resulting edge. Images with a sharp contrast between the inside and the outside of the hole were obtained thanks to the opacity of the mercury film. Then, the dewetting velocity was determined by fitting a line onto the measured radii as a function of time. Uncertainty was typically in the order of 2%.

In the few experiments where the form of the hole was too altered to be fitted by a circle, the dewetting velocity could be estimated by averaging the receding front velocity in several radial directions.

Results

Since the spreading parameter, S, is negative and e is smaller than the critical thickness e_c, the mercury films are metastable and dewet when a hole larger than the critical nucleation radius R_c is initiated (R_c is of the order of e [1]). In the next paragraphs, we investigate the dewetting dynamics of the mercury films, *i.e.*, the form and the evolution of the dewetting hole and the variations of the dewetting velocity as a function of the operating parameters.

Dewetting hole

In most experiments, the dewetting hole is surprisingly circular, as illustrated by the first and third pictures of Fig. 3, and the center of the circle remains stationary during dewetting (we verified this point carefully and found that the tip of the rode used to perforate the film and seen on the pictures of Fig. 3 may slightly move during the dewetting): this very low level of hysteresis is attributed to the large equilibrium contact angle and to the high interfacial energy of the mercury whatever the external phase is. Nevertheless, in few experiments, we observe dewetting holes whose shape is altered due to interactions of the contact line with defects at the solid surface, as shown in the second picture of Fig. 3: the shape of these holes concords with the shape of the dewetting holes reported by Redon.[21]

Last, in some experiments characterized both by a large viscosity ratio, $\lambda \gg 1$, and a low film thickness, the edge of the dewetting hole appeared jagged at multiple scales (see the fourth picture in Fig. 3): from our point of view, this phenomenon is not associated with hysteresis. A more probable explanation is the development of Saffman-Taylor instabilities since the rim consisting of a low-viscosity liquid is locally pushing forward a more viscous fluid, *i.e.*, the external phase. It differs from the rim instability reported by Reyssat and Quéré [15,22] for the bursting of suspended fluid films in an external viscous liquid phase. In the latter case, the holes look circular with regularly spaced sharp tips. The mechanism proposed by Reyssat and Quéré is the following: as the rim is similar to a cylinder, it is subject to the Rayleigh-Plateau instability and tends to transform into

a series of regularly spaced beads. These beads move slower than the main retraction front (since they experience a larger Stokes drag) and are sucked into sharp tips by selective withdrawal.[23,24] This scenario is unlikely in the present experiments. Indeed, we did not observe evidences of the Rayleigh-Plateau instability at smaller viscosity ratios when the instability should grow faster. Furthermore, the capillary number $\mathrm{Ca} = \eta_B V/\gamma_{AB}$ (which varies between $5\ 10^{-4}$ and 10^{-1} for ethanol and M100000 as the external phase, respectively) is systematically much lower than the selective withdrawal threshold (slightly greater than 1).[22,24] It should be also noted that the present instability is very different from the rim instability in the fast inertial regime of soap film bursting:[25] in the latter case, the indentation of the rim and its subsequent breaking into droplets is due to a combination of Kelvin-Helmholtz and Rayleigh-Taylor type instabilities. Unless otherwise stated, the experiments characterized by a non circular dewetting hole will not be taken into account later in the present paper.

Except in inertial regime with hydraulic shock, the shape of the surrounding rim appears asymmetric: the slope of the advancing front is slighter than the receding front. These observations concord with the measurements of Buguin *et al.*[2] in inertial regime and of Andrieux[26] in viscous regime. We expect a steeper advancing front, closer to the receding front slope, for significantly smaller thicknesses than the film thicknesses we could achieve in the present experiments.

Dewetting velocity

In the experiments where the dewetting hole is circular, the velocity of the receding front (*i.e.*, the dewetting velocity) is unambiguously defined by $V = dR/dt$. Measurements show that velocity remains constant during the dewetting process for all experiments, regardless of film thickness and external phase viscosity, *i.e.*, for any regime of dewetting (inertial, visco-inertial or viscous). Fig. 4 represents the variations in the radius of the hole, R, as a function of time for ethanol, M1000 (1 Pa.s) and M100000 (100 Pa.s) silicone oils as the external phase. We see that the variations of R are perfectly linear.

The mercury dewetting velocity varies between 0.2 $\mathrm{m.s^{-1}}$ in air ($\lambda = 10^{-2}$) or in ethanol

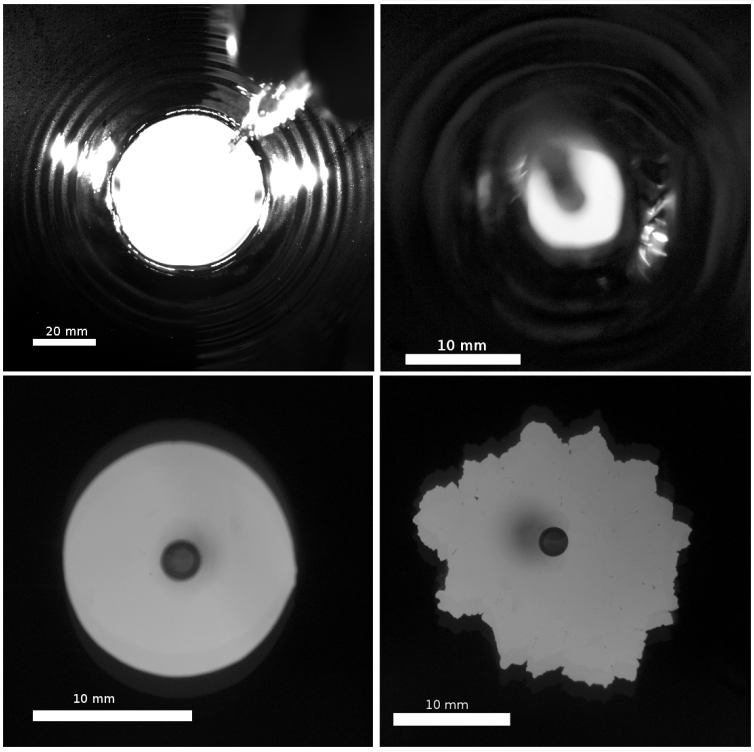

Figure 3: View of an expanding hole in a liquid film of mercury intercalated between a glass slab and an external phase. First picture: top view with air as the external phase (the glass slab was exceptionally a square 100 mm in width, the thickness of the film was equal to 0.55 mm, the dewetting velocity to 0.173 m.s^{-1} and the wave length of the ripples to 2.7 ± 0.1 mm). Second picture: top view with M3 silicone oil as the external phase (the thickness of the film was equal to 0.81 mm, the dewetting velocity to 0.102 m.s^{-1} and the wave length of the ripples to 3.1 ± 0.2 mm). Third picture: bottom view with M1000 silicone oil (the thickness of the film was equal to $e = 1.08$ mm and the dewetting velocity to 1.56 10^{-2} m.s^{-1}). Fourth picture: bottom view with M10000 silicone oil (the thickness of the film was equal to 0.45 mm, the edge of the dewetting hole appears strongly distorted probably due to the development of Saffman-Taylor instabilities).

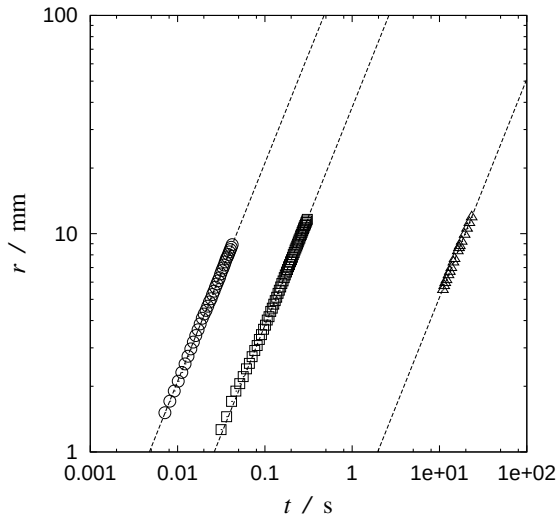

Figure 4: Variations in the hole radius as a function of time for a film 0.64 mm in thickness covered with ethanol (circles), for a film 0.41 mm in thickness covered with M1000 silicone oil (squares) and for a film 0.89 mm in thickness covered with M100000 silicone oil (triangles). The slope of the fitted dashed lines is equal to 1.

($\lambda = 0.8$) down to 5 10^{-4} m.s^{-1} in the most viscous silicone oil ($\lambda = 6\ 10^4$). Thus, the Reynolds number, Re_A, of the mercury film varies typically from 1700 down to 4 and the Reynolds number, Re_B, of the external phase (ethanol or silicone oil) from 150 down to 5 10^{-6} (in the definition of both Reynolds numbers, we use the native film thickness as the characteristic length). When both Reynolds numbers, Re_A and Re_B, are large, the dewetting is inertial. In this regime, for the lowest viscosity ratios (*i.e.*, air, ethanol and M3 silicone oil as the external phase), we observed ripples emitted by the rim. The second (resp. third) picture in Fig. 3 shows such ripples in the case of mercury intercalated between glass and air (resp. M3 silicone oil). These waves are a signature of an hydraulic shock and will be further analyzed in the next section.

We have studied the effect of the film thickness on the dewetting velocity for different values of the viscosity ratio. The variations of V as a function of e are presented in Fig. 5 for ethanol ($\lambda = 0.7$), M100 ($\lambda = 65$) and M1000 silicone oil ($\lambda = 650$) as the external phase. We see that the velocity V follows decreasing functions of e. The decreasing shape of V observed with ethanol is in line with previous measurements in the inertial regime of dewetting.[2,6] Furthermore, at a given film thickness e, the velocity V in Fig. 5 is lower for increasing external phase viscosity;

dissipation by shear in the external liquid phase is obviously the responsible phenomenon.

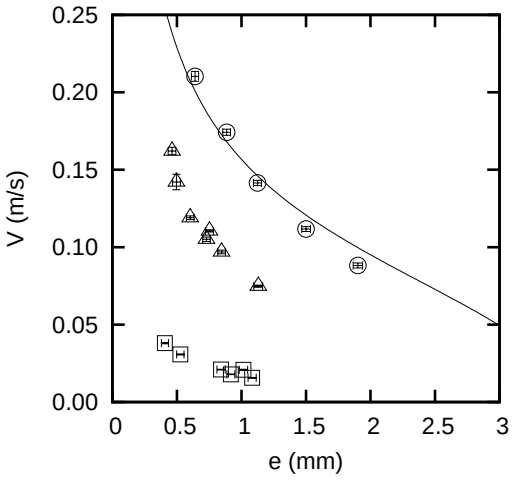

Figure 5: Dewetting velocity as a function of the thickness of the mercury film, with ethanol (circles), M100 silicone oil (triangles) and M1000 silicone oil (squares) as the external fluid phase. The continuous line is the theoretical velocity $(|\tilde{S}_D|/\rho_A e)^{1/2}$ where the dynamic spreading parameter, $\tilde{S}_D$, is half of the static value.

Finally, experiments were done with the different external phases for reduced film thicknesses $e^\sharp = e/\kappa^{-1}$ close to 0.4. The reduced dewetting velocities $V^\sharp = V\ (|\tilde{S}|/(\rho_A e))^{-1/2}$ interpolated at $e^\sharp = 0.4$ are plotted in Fig. 6 as a function of the reduced external phase viscosity $\eta^\sharp = \eta_B\ (|\tilde{S}|\rho_A e))^{-1/2}$. Two asymptotic behaviours are experimentally evidenced in this Figure: the experimental reduced velocity appears constant in the limit $\eta_B^\sharp \ll 1$. This is the inertial regime. In the limit $\eta_B^\sharp \gg 1$, the reduced velocity scales as the inverse of the reduced external phase viscosity. This is the viscous regime. In the next section, we propose a model which accounts for each regime.

Model

Inertial regime

In this regime, the viscous effects in mercury and in the external phase B are negligible compared to the inertial effects. Then, Eq. 2 reduces to $dP/dt = F_d$. The momentum of the moving rim

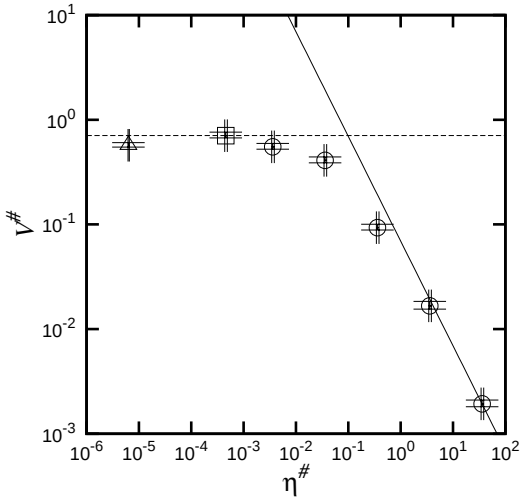

Figure 6: Reduced velocity of dewetting as a function of the reduced viscosity of the external fluid phase for mercury films intercalated between glass and air (square), ethanol (triangle) or silicone oil (circles). The reduced dewetting velocities are interpolated at the reduced film thickness $e^{\sharp} = 0.4$. Horizontal, dotted line: the inertial limit $V^{\sharp} \cong \frac{1}{\sqrt{2}}$ corresponding to a dynamical spreading parameter equal to half of its static value. Plain line: velocity law $V^{\sharp} = \left(\frac{\gamma_{AB}}{k_B|\tilde{S}|}\right) \frac{1}{\eta_B^{\sharp}}$ with $k_B = 8$.

is equal to $P = M_e(t)V$ where $M_e(t)$ is the effective mass of the rim, *i.e.*, the sum of the mass of the rim, $M(t)$, and of the added mass due to the surrounding liquid B. Within the limit of low density ratios, $\rho_B/\rho_A \ll 1$, we may assume that $M_e(t) \cong M(t)$. This assumption holds for the experiments reported in the present paper since they were performed with mercury and light surrounding liquids, *i.e.*, $\rho_B/\rho_A \cong 10^{-1}$. From mass conservation, the mass of the rim is equal to $M(t) = \pi R^2(t) e \rho_A$. The driving force at time t reads: $F_d(t) = 2\pi R(t)|\tilde{S}|$. Since the hole grows at constant velocity $V = dR/dt$, Culick's law, *i.e.*, Eq. 4, is formally recovered in the specific case of a low-viscosity intercalated film.

Fig. 5 shows that the data associated with the dewetting of mercury sandwiched between glass and ethanol are well fitted by Culick's law, Eq. 4, if the spreading parameter $\tilde{S}$ is halved. These results are in line with the findings of Buguin *et al.*:[2] they studied the dewetting of water between glass covered by octadecyltrichlorosilane and air in the inertial regime and introduced a so-called dynamic spreading parameter $\tilde{S}_D$ equal to half of the static spreading parameter $\tilde{S}$ to fit Culick's law to their data. This means that about 50% of the energy released during dewetting is lost in

another process besides being converted into kinetic energy of the rim.[1] So far, this dissipation process has not yet been clearly identified.[1]

Besides, Buguin *et al.*[2] highlighted a bifurcation at a critical value of the Froude number. The Froude number, Fr, characterizing the dewetting process is defined as the ratio of the velocity of the advancing front V_N (see point N in Fig. 1) to the velocity of the gravity waves in shallow water $(ge)^{1/2}$. When Fr > 1, the film flow is supercritical in the referential of the advancing front N and the advancing front is a shallow water shock as first proposed by Brochard and de Gennes,[27] similar to the hydraulic jump observed at the bottom of a sink. This shock is preceded by ripples. The phase velocity, c_φ, of the ripples is equal to the velocity of the advancing front V_N[2,28] and their wavelength, l, satisfy the dispersion relation of linear capillary-gravity periodic waves, namely:[29]

$$c_\varphi^2 = \frac{g}{k}\left(1+(\kappa^{-1}k)^2\right)\tanh(ke) \tag{6}$$

where k is the wave number given by $k = 2\pi/l$. When Fr < 1, the film flow is subcritical in the referential of the advancing front and there is no shock and no ripples associated with.

Such a bifurcation is also expected for the inertial dewetting of mercury covered by an external liquid layer. According to Dias and Vanden-Broeck,[30] who studied theoretically two-layers hydraulic falls, it should occur at the critical Froude number $\mathrm{Fr}_{\mathrm{bif}}$ defined as:

$$\mathrm{Fr}_{\mathrm{bif}} = \left(\frac{\beta\,(1-\rho)}{\beta+\rho}\right)^{1/2} \tag{7}$$

where $\rho = \rho_B/\rho_A$ is the ratio of the fluid densities, $\beta = h/e$ the ratio of the fluid-layer thicknesses and h is the thickness of the external phase layer.

We infer that the ripples emitted in front of the rim (when the Froude number is supercritical) satisfy the dispersion relation for linear capillary-gravity periodic waves in a two-layer system in the presence of a free surface. The dispersion relation has been established by Mohapatra *et al.*[31] It is quadratic in c_φ^2 and the roots are:

$$c_{\varphi\pm}^2 = \left(\frac{g}{k}\right) \frac{B \pm \left(B^2 - 4AC\right)^{1/2}}{2A} \tag{8}$$

where

$$A = \rho + \coth(kh)\coth(ke) \tag{9}$$

$$B = (1-\rho)(\kappa^{-2}k^2+1)\coth(kh) + (\kappa'^{-2}k^2+1)\left(\rho\coth(kh) + coth(ke)\right) \tag{10}$$

$$C = (\kappa'^{-2}k^2+1)(\kappa^{-2}k^2+1)(1-\rho) \tag{11}$$

In Eq. 8, the subscript with + sign (resp. - sign) refers to waves in the free surface mode (resp. in the interfacial or internal mode). κ'^{-1} is the capillary length associated with the free interface, *i.e.*, between the external liquid layer and the air. It is given by $\kappa'^{-1} = (\gamma_B/\rho_B g)^{1/2}$.

In the present experiments, we observed ripples for the lowest viscosity ratios, *i.e.*, for air, ethanol and M3 silicone oil as the external phase. The first (resp. second) picture in Fig. 3 shows such ripples in the case of mercury intercalated between glass and air (resp. mercury between glass and M3 silicone oil). The film thickness was equal to $e = 0.55$ mm (resp. $e = 0.81$ mm), the measured dewetting velocity was equal to $V = 0.173$ m.s^{-1} (resp. $V = 0.102$ m.s^{-1}), the measured phase velocity of the ripples to $c_\varphi = 0.227$ m.s^{-1} (resp. $c_\varphi = 0.167$ m.s^{-1}) and the measured wavelength to $l = 2.7 \pm 0.1$ mm (resp. $l = 3.2 \pm 0.2$ mm). We could not measure the velocity, V_N, of the advancing front. However, we know that V_N is necessary greater than the velocity V_M of the receding front, *i.e.*, the dewetting velocity. We deduce that Fr > 2.4 in the glass/mercury/air experiment of the first picture (resp. Fr > 1.15 in the glass/mercury/M3 experiment of the second picture): the dewetting is supercritical since the critical Froude number is equal to $\mathrm{Fr}_{\mathrm{bif}} = 1$ (resp. $\mathrm{Fr}_{\mathrm{bif}} = 0.97$). The computation of the phase velocity from Eq. 6 gives $c_\varphi = 0.274$ m.s^{-1} for the glass/mercury/air experiment. For the glass/mercury/M3 system, we compute the phase velocity from Eq. 8: the velocity of the waves in the free surface mode is equal to $c_{\varphi+} = 0.239$ m.s^{-1} and the velocity of the waves in the interfacial mode to $c_{\varphi-} = 0.210$ m.s^{-1}: we conclude that

the ripples are more probably waves in the interfacial mode. It can be noticed that the theoretical values of c_φ and $c_{\varphi-}$ are slightly greater than the experimental ones: first of all, it is attributed to the contamination of the mercury surface by some surfactant impurities since the mercury was not handled *in vacuo* or in an inert gas.[32] Second, non-linear effects, appearing if the amplitude of the waves is not small compared to the mercury-film thickness, may also be responsible for this discrepancy.

Viscous regime

In the viscous regime, the motion of the rim is controlled by the balance between the capillary forces F_d and the viscous forces F_v. To derive the velocity of the rim, we follow the argument originally developed by Redon *et al.*[3] We first suppose that $e \ll e_c$ and study the dewetting dynamics of the film when $R \gg e, R_c$. The rim extends from point M at the contact line of the receding front to point N at the advancing front (see Fig. 1). The width of the rim is denoted $l(t)$. It is assumed that the vicinity of the contact line can be described as a wedge with a well-defined dynamic contact angle θ_D. We are aware that there are some deviations from this wedge shape as pointed by Voinov, Cox and de Gennes *et al.*[34–36] However, it is expected that the main features of the dewetting dynamics can be understood from the wedge approximation. The pressure in the rim is expected to equilibrate rapidly: according to Laplace law, the rim cross section is thus a portion of a circle. This implies that the dynamic contact angle at point M and the angle at point N are equal. There are some deviations from the arc shape (weak dissymmetry between the receding and advancing fronts) as pointed out by Andrieu[26] but they are ignored in the present approach.

Within the limit of small contact angles, the equation of conservation of volume applied to the rim reads:[1,33] $\pi R^2 e \simeq \pi R l^2 \theta_D$. It is deduced that $l(t)$ scales as $R^{1/2}$, *i.e.*, as $t^{1/2}$. Since dl/dt is small compared with $V = dR/dt$, the velocity of the advancing front V_N may be assimilated to the velocity of the receding front $V_M = V$ and the changes in the geometry of the rim are slow with respect to V.

To express the dissipative force F_v, it is assumed that (i) the viscous dissipation in the liquids

dominates over all dissipation processes acting during the dewetting (ii) it occurs mainly near the edges M and N (iii) the advancing front N is assimilated to a pseudo-contact line moving on the solid S pre-covered by the mercury film (A) of thickness e, (iv) the thickness, e, of the film A and the width, l, of the rim are much lower than the thickness, h, of the external phase B.

Under these assumptions, for finite variation range of θ_D, F_v may be expressed as:

$$F_v = k_{AM}\eta_A\theta_D^{\alpha}V_M + k_{BM}\eta_B\theta_D^{\beta}V_M + k_{AN}\eta_A\theta_D^{\alpha}V_N + k_{BN}\eta_B\theta_D^{\beta}V_N \tag{12}$$

The first and the second terms (resp. the third and fourth terms) of the right-hand side of Eq. 12 are associated with the dissipation in the film A and in the external phase B near edge M (resp. edge N). k_{AM} and k_{BM} are logarithmic factors, involving a macroscopic cutoff of the order of the width of the rim l and a microscopic cutoff of the order of a molecular size, a and b, associated with liquids A and B, respectively: k_{AM} and k_{BM} scale as $\ln l/a$ and $\ln l/b$, respectively. Reported values of k_{AM} and k_{BM} are of the order of 10. At the N edge, k_{AN} and k_{BN} rather scale as $\ln l/e$ since the advancing front N is sliding on a solid pre-covered by a liquid film of thickness e. k_{AN} and k_{BN} are of the order of unity. According to Huh and Scriven's calculations[5] and Brochard-Wyart and de Gennes analysis,[10] the exponents α and β are equal to $\alpha = -1$ and $\beta = 2$, respectively, in the limit of small contact angle θ_D satisfying the relation $\theta_D > (\eta_A/\eta_B)^{1/3}$. Whereas the value $\alpha = -1$ is widely confirmed experimentally (at least when fluid B is a gas), very few studies focus on the experimental determination of β. Debregeas and Brochard-Wyart[18] approached this problem in their study of the displacement of a film of air lying between a glass slide silanized with octadecyltrichlorosilane, they found a weaker dependence of the external phase viscous friction on the dynamic contact angle: in their experiments, it rather scales as $\theta_D^{0.7}$, *i.e.*, $\beta = 0.7$. This value has been further found consistent with Martin's results on the viscous dewetting of intercalated films.[11]

Let us assume that the dynamic contact angle θ_D satisfies the relation

$$\theta_D \gg \left(\frac{\eta_A}{\eta_B}\right)^{\frac{1}{\beta-\alpha}}, \tag{13}$$

This condition should hold for systems characterized by large equilibrium contact angle and for large enough external phase viscosities. Then F_v simplifies to give:

$$F_v = k_{BM}\eta_B\theta_D^{\beta}V_M + k_{BN}\eta_B\theta_D^{\beta}V_N \tag{14}$$

To derive the dewetting velocity, we add the force balance at the receding contact line M to Eq. 2. Hence, we obtain the following system of equations, respectively:

$$k_{BM}\eta_B\theta_D^{\beta}V_M + k_{BN}\eta_B\theta_D^{\beta}V_N = \gamma_{AB}(1-\cos\theta_E) \tag{15}$$

$$k_{BM}\eta_B\theta_D^{\beta}V_M = \gamma_{AB}(\cos\theta_D - \cos\theta_E) \tag{16}$$

It should be noted that $F_d = |\tilde{S}|$ has been approximated by $|S| = \gamma_{AB}(1-\cos\theta_E)$ in the right-hand side of Eq. 15 since $e \ll e_c$. The right-hand side of Eq. 16 represents the uncompensated Young force acting on the receding contact line.

Taking into account that $V_N \approx V_M = V$, Eq. 15 and 16 lead to:

$$\cos\theta_D = \frac{\cos\theta_E + D}{1+D} \tag{17}$$

with $D = \frac{k_{BM}}{k_{BN}}$. Since $k_{BM} \sim \ln l/a \sim 10$ and $k_{BN} \sim \ln l/e \sim 1$, $D \sim 10$ and it is deduced that even for large values of the equilibrium contact angle θ_E, $\cos\theta_D \sim 1$, thus, in the viscous regime, θ_D is expected to remain much smaller than unity. θ_D is given by $\theta_D \approx 2(D+1)^{-1/2}$ for θ_E close to π.

Since $\theta_D \ll 1$, the dewetting velocity reads:

$$V \approx \frac{\gamma_{AB}}{k_B\eta_B} \tag{18}$$

The factor k_B depends on k_{BN}, D and β and scales as $k_{BN}\,(1+D)^{1-\frac{\beta}{2}}$. The dimensionless form of relation 18, *i.e.*, $V^\sharp \approx \left(\frac{\gamma_{AB}}{k_B|\tilde{S}|}\right)\,\frac{1}{\eta_B^\sharp}$, is represented in Fig. 6 with $k_B = 8$: the experimental points are observed to approach this law at large $\eta_B^\sharp$.

We have assumed that $e \ll e_c$. As e increases, $\cos\theta_D$ decreases from $\cos\theta_D \sim 1$ to $\cos\theta_D = \cos\theta_E \sim -1$ for $e \to e_c$ where the driving force $|\tilde{S}| = 0$. To calculate θ_D, we must add in Eq. 15 right-hand side, the gravity force $-\frac{1}{2}(\rho_A - \rho_B)ge^2 = -\frac{1}{2}\gamma_{AB}\kappa^2 e^2$. It leads to:

$$\cos\theta_D = \cos\theta_E + \frac{D}{D+1}\left\{\frac{1}{2}\kappa^2\left(e_c^2 - e^2\right)\right\} \tag{19}$$

$$\eta_B D k_{BN}\theta_D^\beta V = \gamma_{AB}\frac{D}{D+1}\left\{\frac{1}{2}\kappa^2\left(e_c^2 - e^2\right)\right\} = \frac{D}{D+1}|\tilde{S}| \tag{20}$$

We check that for $e \to 0$, $\cos\theta_D \sim 1$ and that for $e = e_c$, $\cos\theta_D = \cos\theta_E$. The velocity will scale as $V \sim |\tilde{S}|/\eta_B$, with a coefficient slightly decreasing as e increases.

We got similar conclusions in the limit $\theta_E \ll 1$. Indeed, in this case, θ_D is given by $\theta_D \approx \theta_E\,(D+1)^{-1/2}$, for $e \ll e_c$. The dewetting velocity reads $V \approx \frac{\gamma_{AB}}{k_B'\eta_B}\theta_E^{2-\beta}$, and k_B' has the same scaling behaviour as k_B.

One can notice that the dewetting of low-viscous films at solid/viscous liquid interfaces follows similar law to the bursting of suspended films of water or air in a viscous environment.[15] In both cases, the characteristic retraction velocity scales as $|S|/\eta_B$ ($|S| = 2\gamma_{AB}$ for a suspended film). However, in the case of a suspended film, there is no contact line (and no viscous dissipation associated with) and the true dependence of the retraction velocity on the external phase viscosity is weaker, *i.e.* $\ln\eta_B/\eta_B$ instead of $1/\eta_B$.[15]

Crossover

The crossover between the inertial and the viscous regimes is found by matching Eq. 4 with Eq. 18. For low-viscosity films of given thickness $e \ll e_c$, the crossover occurs at $\eta_B^* \approx \frac{1}{k_B}(2\rho_A e\gamma_{AB})^{1/2}$ for θ_E close to π.

It should be mentioned that the crossover occurs at $\eta_B^* \approx \frac{2}{k_B'} \theta_E^{1-\beta} (\rho_A e \gamma_{AB})^{1/2}$ for $\theta_E \ll 1$. More generally, for any film thickness $e < e_c$ and any equilibrium contact angle, the crossover is expected to occur at $\eta_B^* \approx (\rho_A e |\tilde{S}|)^{1/2}$ where the prefactor has been omitted.

In the crossover region, the regime of dewetting is visco-inertial. In the present study, the glass/mercury/M100 and glass/mercury/M1000 systems typically fall under this regime. The variations of V as a function of e are presented in Fig. 5 for both systems. It appears that the dewetting velocity scales as $e^{-\frac{1}{2}}$ but the proportionality coefficient strongly depends on the viscosity of the external phase. Indeed, as η_B increases, the share of released energy being lost by viscous dissipation also increases.

Conclusion

Studies dealing with wetting, dewetting or more generally with the contact line displacement of a solid/liquid/liquid system are rare compared with the solid/liquid/gas configuration.

In the present work, we focused on the dewetting of low-viscosity liquid film intercalated between a solid substrate and an external non-miscible liquid phase within the limit of large equilibrium contact angle: we performed dewetting experiments with mercury intercalated between floated glass and a series of non-miscible external phase, *i.e.*, air, ethanol and silicone oils. The viscosity of the external phase was varied over seven orders of magnitude.

The mercury films dewet by the nucleation and growth of a hole surrounded by a rim which collects the mercury. In most experiments, the hole is circular. The dewetting velocity, $V = dR/dt$, remains constant during the dewetting process, regardless of film thickness and external phase viscosity.

We observe a transition between two regimes of dewetting at the threshold viscosity $\eta_B^* \approx (\rho_A e |\tilde{S}|)^{1/2}$. For $\eta_B \ll \eta_B^*$, the regime is inertial. The velocity of dewetting is ruled by Culick's law, $V \approx (|\tilde{S}_D|/(\rho_A e))^{1/2}$, where $\tilde{S}_D$ is the dynamic spreading coefficient equal to about half of its static value, $\tilde{S}$. Furthermore, the inertial regime of dewetting presents a bifurcation at a critical

Froude number, $\mathrm{Fr}_{\mathrm{bif}}$. When the Froude number characterizing the dewetting process is greater than $\mathrm{Fr}_{\mathrm{bif}}$, there is an hydraulic shock and ripples are emitted in front of the rim. Otherwise, there is no shock and no ripples are seen. We analyzed the ripples in the frame of the linearized theory of water waves and we found that they satisfy the dispersion relation for linear capillary-gravity periodic waves in a two-layer system in the presence of a free surface.

For $\eta_B \gg \eta_B^*$, the regime of dewetting is viscous. The dewetting velocity scales as $V \sim |\tilde{S}|/\eta_B$. We interpret this regime by a balance between the surface energy released during dewetting and the viscous dissipation in the external phase near the edges of the rim. In this regime, we observed, for the lower film thicknesses and the higher viscosity ratios ($\lambda = \eta_B/\eta_A \gg 1$), the development of Saffman-Taylor-type instabilities which lead to a dewetting hole distorted at multiple scales. To our knowledge, such instabilities during dewetting have not yet been reported in the literature and need to be further investigated.

Acknowledgement

We thank F. Dias for fruitful exchanges concerning interfacial waves. This research was supported by Agence Nationale de la Recherche as part of the CIREM project (grant number ANR06 MAT-PRO 0005).

Supporting Information Available

The dewetting of mercury films sandwitched between a glass slab and an external phase is illustrated by four movies corresponding to the four pictures of Fig. 3, respectively.

This material is available free of charge via the Internet at `http://pubs.acs.org/`.

Appendix. Film thickness measurement by a gravimetric procedure

Let us first express the film thickness e_0 as a function of the difference Δm in weighing scale reading before and after the dewetting, when ignoring the meniscus at the edge of the glass slab.

On the grounds of volume conservation and hydrostatic equilibrium, e_0 is given by:

$$e_0 = \left[\left(1 + \frac{\rho_B}{\rho_A - \rho_B}\left(1 - \frac{\Sigma_s}{\Sigma_c}\right)\right)(\Sigma_d + \Sigma_r) + \frac{\rho_A}{\rho_A - \rho_B}(\Sigma_c - \Sigma_s)\right]\frac{\Delta m}{\Sigma_d \Sigma_s \rho_A}, \tag{21}$$

where Σ_s is the surface area of the glass slab while Σ_c, Σ_r and Σ_d are the horizontal cross-sectional areas of the glass slab cell, the reservoir and the weighing scale dish respectively (these horizontal cross sections are properly corrected to account for the cross section of the siphon pipes). Accounting for the meniscus formed at the edge of the slab, volume conservation and hydrostatic equilibrium lead to the following equation for the actual film thickness e:

$$e + \frac{p}{\Sigma_s} s(e + \delta) = e_0, \tag{22}$$

where e_0 is the approximate thickness of Eq. 21. The function s is the cross-sectional area of the meniscus at the edge of the glass slab (Fig. 7), defined for $0 < z < \sqrt{2}\ \kappa^{-1}$ by $s(z) = \kappa^{-1}\ z\ \left(1 - \frac{\kappa^2 z^2}{4}\right)^{1/2}$. The variable p is the total perimeter of the glass slab and δ is the height difference of the upper phase/mercury interface in the glass slab cell before and after the dewetting:

$$\delta = \frac{\Sigma_c \rho_A + (\Sigma_d + \Sigma_r)\rho_B}{\rho_A - \rho_B}\ \frac{\Delta m}{\Sigma_c \Sigma_d \rho_A}. \tag{23}$$

The thickness e was determined by solving Eq. 22 by the Newton-Raphson method. The meniscus contribution had to be accounted for since the value of e could be 15% less than e_0.

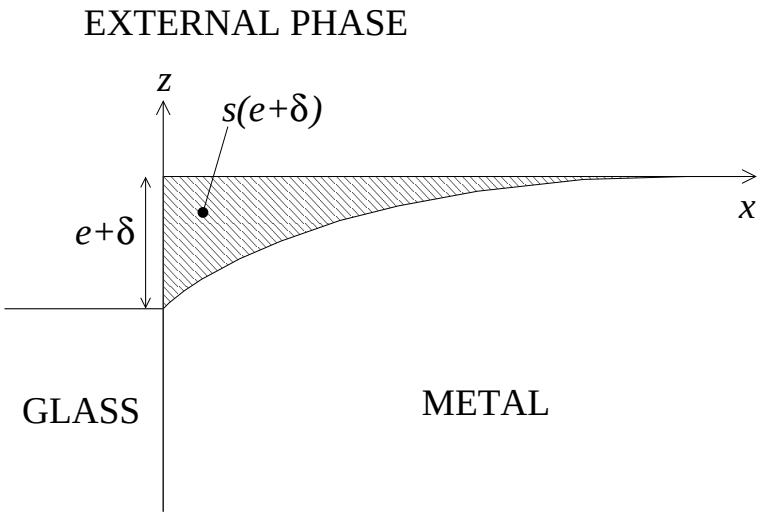

Figure 7: The shape of the external phase/liquid metal interface at the edge of the glass surface after dewetting. The hatched area is the cross section $s(e+\delta)$.

References

(1) de Gennes, P.G.; Brochard-Wyard, F.; Quéré, D. *Gouttes, bulles, perles et ondes*, 1st ed.; Belin: Paris, 2002.

(2) Buguin, A.; Vovelle, L.; Brochard-Wyart, F. Shocks in Inertial Dewetting *Phys. Rev. Lett.* **1999**, *83*, 1183-1186.

(3) Redon, C.; Brochard-Wyart, F.; Rondelez, F. Dynamics of Dewetting *Phys. Rev. Lett.* **1991**, *66*, 715-718.

(4) Culick, F.E.C. Comments on a Ruptured Soap Film *J. Appl. Phys.* **1960**, *31*, 1128-1129.

(5) Huh, C.; Scriven, L.E. Hydrodynamic Model of Steady Movement of a Solid/Liquid/Fluid Contact Line *J. Colloid Interface Sci.* **1971**, *35*, 85-101.

(6) Andrieu, C.; Sykes, C.; Brochard-Wyart, F. Dynamics of Fast Dewetting on Model Solid Substrates *J. Adhesion* **1996**, *58*, 15-24.

(7) Shull, K.R.; Karis, T.E. Dewetting Dynamics for Large Equilibrium Contact Angles *Langmuir* **1994**, *10*, 334-339.

(8) Haidara, H.; Vonna, L.; Schultz, J. Instability and Dewetting of Confined Thin Liquid Films in Nonmiscible External Bulk Fluids (Water and Aqueous Surfactant Solutions): Experiments versus Theoretical Predictions *Langmuir* **1998**, *14*, 3425-3434.

(9) Joanny, J.F.; Andelman, D. Steady-State Motion of a Liquid/Liquid/Solid Contact Line *J. Colloid Interface Sci.* **1987**, *119*, 451-458.

(10) Brochard-Wyart, F.; de Gennes, P.G. Spreading of a Drop between a Solid and a Viscous Polymer *Langmuir* **1994**, *10*, 2440-2443.

(11) Martin, P. *Démouillage d'un Film Liquide Intercalé entre un Solide et un Milieu Déformable* Thesis, University of Paris VI, 1997.

(12) Martin, P.; Brochard-Wyart, F. Dewetting at Soft Interfaces *Phys. Rev. Lett.* **1998**, *80*, 3296-3299.

(13) Brochard-Wyart, F.; de Gennes, P.G. Dewetting of a Water Film between a Solid and a Rubber *J. Phys.: Condens. Matter* **1994**, *6*, A9-A12.

(14) Joanny, J.F.; de Gennes, P.G. Bursting of a soap film in a viscous environment *Physica A* **1987**, *147*, 238-255.

(15) Reyssat, E.; Quéré, D. Bursting of a fluid film in a viscous environment *Europhys. Lett.* **2006**, *76*, 236-242.

(16) Adamson, A.W. *Physical Chemistry of Surfaces,* 5^{th} ed.; Wiley: New York, 1990.

(17) Ishakoglu, A.; Baytas, A.F. The Influence of Contact Angle on Capillary Pressure-saturation Relations in a Porous Medium including Various Liquids *Int. J. Eng. Sci.* **2005**, *43*, 744-755.

(18) Debrégeas, G.; Brochard-Wyart, F. Nucleation Radius and Growth of a Liquid Meniscus *J. Colloid Interface Sci.* **1997**, *190*, 134-141.

(19) Reiter, G.; Schwerdtfeger, K. Characteristics of Entrainment at Liquid Liquid Interfaces due to Rising Bubbles *ISIJ Int.* **1992**, *32*, 50-56.

(20) Bartell, F.E.; Osterhof, H.J. The Measurement of Adhesion Tension Solid against Liquid *Colloid Symp. Monogr.*, **1927**, *5*, 113-134.

(21) Redon, C. *Dynamique du Mouillage et du Démouillage de Surfaces Modèles* Thesis, University of Paris VI, 1991.

(22) Reyssat, E. *Gouttes, Films et Jets: quand les Ecoulements Modèlent les Interfaces* Thesis, University of Paris VII, 2007.

(23) Cohen, I.; Nagel, S.R. Scaling at the Selective Withdrawal Transition through a Tube Suspended above the Fluid Surface *Phys. Rev. Lett.*, **2002**, *88*, 074501(4).

(24) Courrech du Pont, S.; Eggers, J. Sink Flow Deforms the Interface Between a Viscous Liquid and Air into a Tip Singularity *Phys. Rev. Lett.*, **2006**, *96*, 034501((4).

(25) Lhuissier, H.; Villermaux, E. Soap Films Burst like Flapping Flags *Phys. Rev. Lett.*, **2009**, *103*, 054501(4).

(26) Andrieu, C. *Angles de Contact et Démouillage* Thesis, University of Paris VI, 1995.

(27) Brochard-Wyart, F.; de Gennes, P.G. Shocks in an Inertial Dewetting Process *C.R. Acad. Sci. Ser. II-B* **1997**, *324*, 257-260.

(28) Brochard-Wyart, F.; Raphael, E.; Vovelle, L. Démouillage en Régime Inertiel: Apparition d'Ondes Capillaires *C.R. Acad. Sci. Ser. II-B* **1995**, *321*, 367-370.

(29) Lamb, H. *Hydrodynamics*, 6^{th} ed.; Cambridge University Press: New York, 1975.

(30) Dias, F.; Vanden-Broeck J.M. Two-layer Hydraulic Falls over an Obstacle *Eur. J. Mech. B Fluids* **2004**, *23*, 879-898.

(31) Mohapatra, S.C.; Karmakar D., Sahoo T. On Capillary Gravity-wave Motion in Two-layer Fluids *J. Eng. Math.* **2011**, *71*, 253-277.

(32) Elliott, T.A.; Wilkinson, M.C. Effect of Base-Metal Impurities on Surface Tension of Mercury *J. Colloid Interface Sci.* **1972**, *40*, 297-304.

(33) Brochard-Wyart, F.; Martin, P.; Redon, C. Liquid-liquid Dewetting *Langmuir* **1993**, *9*, 3682-3690.

(34) Voinov, O.V. Hydrodynamics of Wetting *Fluid Dyn.* **1976**, *11*, 714-721.

(35) Cox, R.G. The Dynamics od the Spreading of Liquids on a Solid Surface. Part 1. Viscous Flow *J. Fluid Mech.* **1986**, *168*, 169-194.

(36) de Gennes, P.G.; Xua, H.; Levinson, P.J. Dynamics of Wetting - Local Contact Angle *J. Fluid Mech.* **1990**, *212*, 55-63.

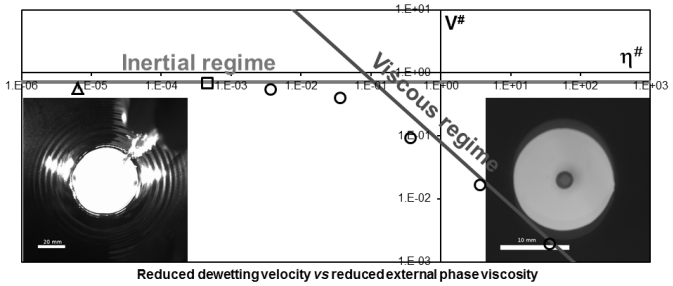

Figure 8: For Table of Contents only